SIMULATIONS OF ECC SAFETY INJECTION FOR SINGLE PHASE AND STRATIFIED PHASE FLOW

Kai Wang, Rong Cai, Wuyue Ren, Suizheng Qiu*, Wenxi Tian, G.H.SU, Ronghua Chen
School of Nuclear Science and Technology, State Key Laboratory of Multiphase Flow in Power Engineering, Xi'an Jiaotong University
Xianning West Rd. 28, Xi'an, Shaanxi 710049, P.R. China
szqiu@mail.xjtu.edu.cn

ABSTRACT
ECC safety injection nozzles are usually placed at the primary circulation pipelines as for the Gen II-plus nuclear reactor. Small Break Loss of Coolant Accident (SBLOCA) may lead to Pressurized Thermal Shock (PTS) on the Reactor Pressure Vessel (RPV) wall. Based on the Emergency Core Cooling (ECC) of a 2nd generation plus PWR, the CFD software CFX was adopted to simulate the thermal mixing phenomenon of the sub-cooled water from safety injection nozzle and high temperature water or steam from the cold leg which later forms into stratified flow. Also the steam-water simulation takes the steam condensation into consideration and steam condensation is characterized by a relatively large interfacial area between the two phases. For simulations of single-phase thermal mixing, the temperature profiles of different points were obtained and agreed well with the experiment. For steam mixing with water, the gas volume profile and the condensation rate of the steam were obtained and compared with the experiment, and the effect of different injection nozzle water velocities were also studied.

KEYWORDS
ECC; Thermal mixing; Stratified flow; Direct contact condensation

1 INTRODUCTION

Complex phenomena may take place when cold water is transported from injection nozzle to the cold leg. The mixing of sub-cooled water and high temperature water can simulate LOCA in PWR. Thermal stress arising from temperature fluctuations in the cooling system of nuclear power plants is almost inevitable. Igarashi et al. (2003) investigated the temperature and velocity distribution in the mixing tee, an in-house direct numerical simulation (DNS) code DINUS-3 was applied to understand the mixing phenomenon. Calculations for the wall jet case showed that the vortices in the wake region caused large temperature fluctuations. Analytical results revealed that three types of vortices generated in the downstream region. Hu and Kazimi (2006) had studied temperature fluctuations caused by thermal mixing in T-junctions using large eddy simulation (LES) turbulence model. Large eddy simulations (LES) were carried out using previously converged Reynolds stress model (RSM) solution as the initial condition. The results showed that the calculated maximum temperatures were somewhat higher than measurements. Seyed Mohammad Hosseini(2006) classified the turbulent jet mechanics in order to examine the flow-field structure under various operating conditions. By comparing the mean velocity distributions, velocity fluctuations, and time-series data, the behaviours of the branch jet are categorized into four types of turbulent jets; the wall jet, the re-attached jet, the turn jet, and the impinging jet. Th. Frank(2010) investigated the turbulent isothermal and thermal mixing phenomena in two different testcase scenarios. He applied ANSYS CFX 11.0 with Reynolds averaging based (U)RANS turbulence models (SST, BSL RSM) as well as with scale-resolving SAS-SST turbulence model in the simulation. One results showed good quantative agreement with the experiment whereas the other showed otherwise.

This work will later deal with the steam from the cold leg mixing with sub-cooled water, of which the experiment has already been conducted. To validate CFD models for numerical simulations of two-phase PTS scenarios, the steam from the safety injection mixing with the sub-cooled water which later forms into stratified flow was studied. Hoehne et al. (2011) used an algebraic interfacial area density (AIAD) model for prediction of counter-current flow limitation (CCFL) in a model of PWR hot leg. Pavel Apanasevich (2013) presented CFD simulations of a steady-state TOPFLOW-PTS air/water experiment and the simulations of a steady-state TOPFLOW-PTS steam/water case with condensation. These CFD simulations were performed with ANSYS FLUENT, ANSYS CFX and NEPTUNE CFD. It was found the simulations of the TOPFLOW-PTS experiments have depicted considerable differences between the codes and the models. However, the previous works mainly focused on a mixing tee, whereas this work is to deal with the safety injection nozzle and cold leg forming a 45 degree angle, not 90ºC. Based on the ECC experiment conducted by our team, the CFD software CFX is applied to study the mixing phenomenon in ECC safety injection.

2 MATHEMATICAL AND PHYSICAL MODELS

This work adopts an Eulerian-Eulerian multiphase model, where the liquid and gas can exist in a single grid and can be distinguished by the volume fraction of each phase. For the single phase thermal mixing of sub-cooled and high temperature water, the k-ε model is introduced in this work. Discusses below are mainly about models used in two-phase constructions.

In the present simulation, CFD methods is applied to solve this three dimensional (3-D) multi-phase flow with phase change. Drag force was modelled by using the Algebraic Interface Area Density (AIAD) model brought out by Hoehne et al.

2.1 AIAD Model and Free Surface Drag Force

Both the liquid and gas phase of the free surface are treated as continuous phase. However, during the mixing period, there can exist bubbles and droplets. It will be much more difficult to simulate two continuous phases and two dispersed phase using sources in the continuous domain. It is noted by Hoehne and Vallée (2010) that the CFD simulation of the free surface can be performed by using the multi-fluid Euler–Euler free surface modelling approach available in ANSYS CFX.

However this approach requires a careful treatment of the interfacial area density and drag force. It makes it reliable to treat the four morphology using different interfacial area density and drag force at different regimes. Egorov (2004) proposed an Algebraic Interfacial Area Density (AIAD) model to solve the above problem.

Totally there are three different morphologies (free surface flow, dispersed bubbles and dispersed droplets), which can be defined by using different blending factor f based on the variation of volume fraction. Each interfacial area density and drag force varies with different volume fraction. That is, when the gas volume fraction is smaller than 0.3 or larger than 0.7, this area is deemed as the bubbly region or the droplet region respectively and the bending factor can be written as

$$f_B = [1 + e^{\alpha_B(\alpha_G - \alpha_{B,limit})}]^{-1} \quad (1)$$

$$f_D = [1 + e^{\alpha_D(\alpha_L - \alpha_{Ds,limit})}]^{-1} \quad (2)$$

When the gas volume fraction is between 0.3 and 0.7, it is regarded as the free surface flow and the bending factor of which can be written as

$$f_{FS} = 1 - f_B - f_D \quad (3)$$

where f_B , f_D , f_{FS} are the blending factor for bubbly, droplet and free surface region, respectively.

When the gas volume fraction is below 0.2, f_B is approximately unity with f_D and f_{FS} being zero. When it is between 0.2 and 0.4, it can be seen as the transitional region between bubbly region and free surface region. Similarly, the free surface and droplet region can be defined accordingly.

Therefore, the total interfacial area density can be written as follows:

$$A = f_{FS}A_{FS} + f_B A_B + f_D A_D \tag{4}$$

More details on the AIAD model can be found in the works of Hoehne et al.

2.2 Heat transfer model

In order to simulate the condensation of steam on the liquid, the phase change model has been applied. The Nusselt number is calculated from the turbulent Reynolds and Prandtl number of liquid using surface renewal theory introduced by Coste et al. (2008):

$$Nu_L = \frac{2}{\sqrt{\pi}} \mathrm{Re}_t \, \mathrm{Pr}^{1/2} \tag{5}$$

2.3 Turbulence equations

The well-known single-phase turbulence models are usually used to model turbulence of the liquid phase in Eulerian–Eulerian multiphase simulations. In the present work, the homogeneous model is applied for the free surface as they are both continuous flow. Here the $k-\varepsilon$ based SST is applied and the model accounts for the transport of the turbulent shear stress and gives highly accurate predictions of the onset and the amount of flow separation under adverse pressure gradients.

3 EXPERIMENT INTRODUCTION AND NUMERICAL DETAILS

3.1 Experiment Introduction

(a)Single Phase (b) Multiple phase

Fig.1 Overall view of the test facility

The experiment setups for the single phase and multiple-phase are not the same and they are presented separately as depicted above. The test sections in the single-phase water test and the multiple-phase water test are not same, and both test sections are presented separately above. The test section for the single phase simulation was made of stainless steel and due to the high pressure(some working cases can be as high as 10MPa), the test facility is not equipped with glass windows. So the velocity profile cannot be acquired by means of PIV or LDV, which means the velocity profile of the simulations cannot be validated against the experiment. The temperatures of the water were measured by thermocouples.

The test section for the multiple-phase was equipped with glass windows to allow visual observation. A vortex meter was used to measure the injected water mass flow rate. The injected steam mass flow rate was measured and controlled using a gas mass flow meter. The temperatures of both the steam and water were measured by thermocouples. However, due to some reasons, the temperature profile will not be

included in this work. The gas volume fraction of one cross-section is measured by γ-ray measuring technology. The gas fraction of the cross-section can be acquired by the amount of the attenuation of the γ-ray.

3.2 Geometry model and measuring points

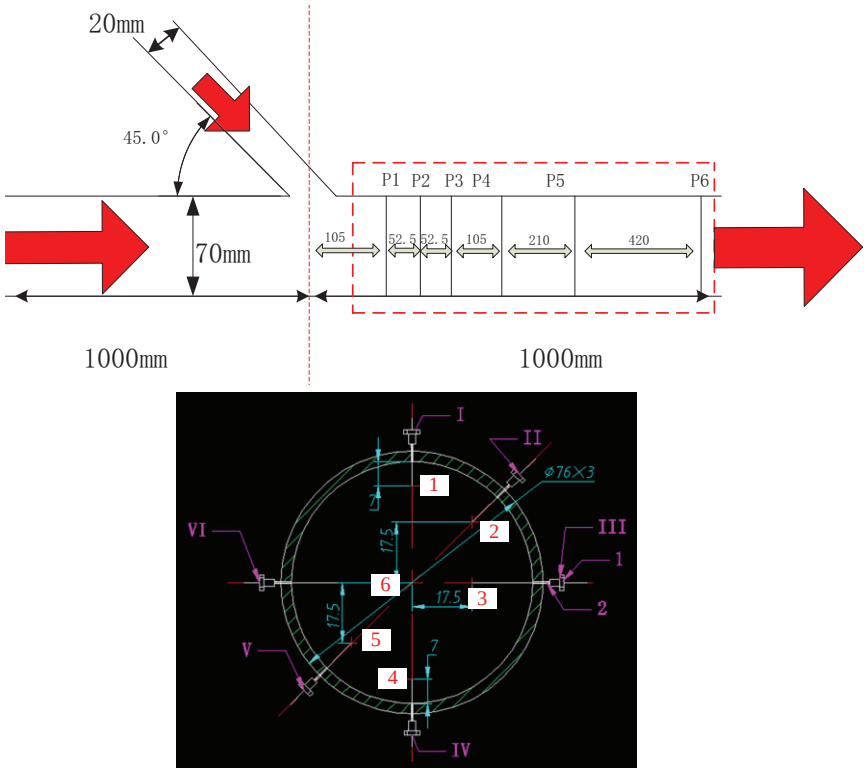

Fig.2. The positions for the measuring planes and relative measuring points positions

The main pipe has a diameter of 70mm and the branch pipe has a diameter of 20mm. There are totally six measuring planes after the mixing area. Plane 4,5,6 has two measuring points, denoted as up point which is 7mm from the top and down point which is 7mm from the bottom, noted that for a more detailed look into the thermal mixing, the plane 1,2 and 3 have 6 measuring points each, making 24 measuring points totally. During the experiment, these points were measured by thermal-couplings. The locations of the planes are shown in Fig. 2. Also the relative measuring point positions are shown at the right.

3.3 Grid independent analysis

Three sets of grid are established to obtain the independent grid which are named as the coarse grid (mesh with 61037 nodes), the medium grid (mesh with 426220 nodes), the fine grid (mesh with 746484 nodes). Water from the safety injection inlet has a mass flow rate of 500kg/h and temperature of 25 ^{O}C, while saturated steam under the local pressure from the injection nozzle has a mass flow rate of 25kg/h. From the results shown in Fig.3, it can be seen that the outlet gas volume fraction fit the experiment well and the medium grid is chosen as the final grid and the coarse grid is used as the initial grid for the medium grid. The chosen grid is with a quality bigger than 0.3 and volume change from 0.8 to 4.

In view of the observed effect of grid size, the simulations have been carried out by using 426220 grid points as shown in Fig.4. The mesh is refined near the wall, and the mesh at the mixing area is also refined. Initial simulations were carried out with a coarse mesh to obtain an initial converged solution

and to obtain an indication of where a high mesh density was needed. However, a dense mesh required additional computational effort. Under-relaxation factors between 0.8 were adopted for all flow quantities. At the pipe outlet, a relative average static pressure of zero was specified. It is noted during the simulations that the y plus varied from 10 to 270.

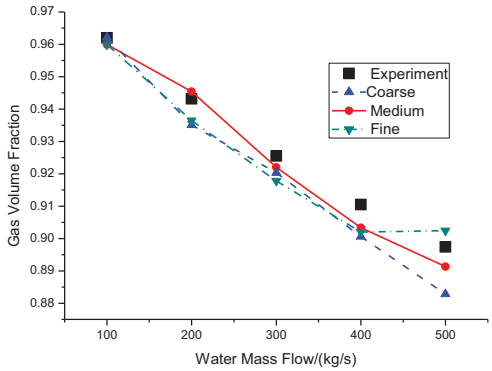

Fig.3. Geometry effect of grid size on the gas volume fraction

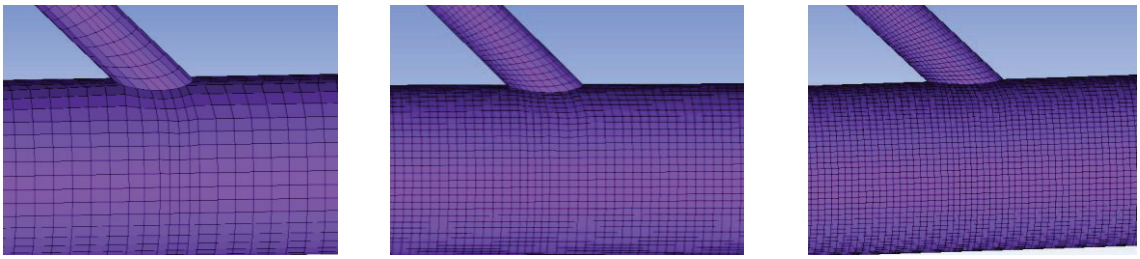

(a) Coarse Grid (b) Medium Grid (c) Fine Grid

Fig.4. Different sets of grid for the simulation

In the simulation of the condensing steam/water flow, steam was supposed to be isothermal (saturated). Therefore, only the energy equation for water was solved. The essential closure law for direct contact condensation (DCC) is the liquid heat transfer coefficient. The steam and water properties varied with pressure and temperature, where IAPWS water tables were used. In the simulations the coupled volume fraction algorithm was chosen. This option allows the implicit coupling of the discretized velocity, pressure and volume fraction equation in order to get the convergence of the calculations in fewer iteration loops. A second order discretization scheme was used to discretize the convective terms in the equations. A second order backward Euler scheme was used to approximate the transient terms.

4 RESULTS AND DISCUSSIONS

4.1 Single Phase Simulation

A research about a mixing tee has been done by Seyed Mohammad Hosseini (2008), and the velocity and the temperature profiles were analysed with some assumptions.

Depending on the momentum/velocity ratio of the entering flows from branch pipe and the main pipe, the turbulent mixing patterns can be further divided into four branch jets such as the wall jet, re-attached jet, turn jet and impinging jet. The types of mixing flow are categorized by using the momentum ratio equation as follows,

$$M_R = \frac{\rho_m V_m^2 (D_m \times D_b)}{\frac{\pi}{4} D_b^2 \rho_b V_b^2} \quad (6)$$

where M_R is the momentum ratio, ρ_m and ρ_b are the fluid densities for the main flow and branch flow, U_m and U_b are the mean velocity of the main and branch flow, D_m and D_b are the main and branch pipe diameters.

By increasing the mass flow from the inlet, M_R increased without changing other parameters. The experiment and the numerical data of Plane 4 are compared in Fig.5.

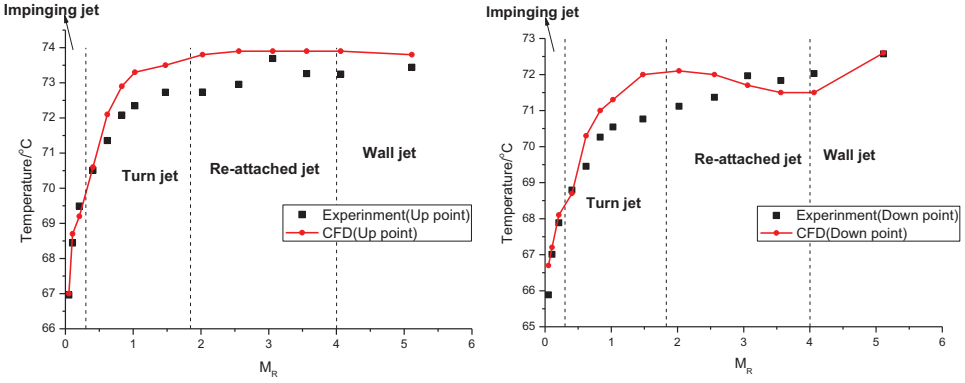

(a) Temperature variation at up point (b) Temperature variation at down point

Fig.5. Comparison of temperature variation calculated and measured values with M_R

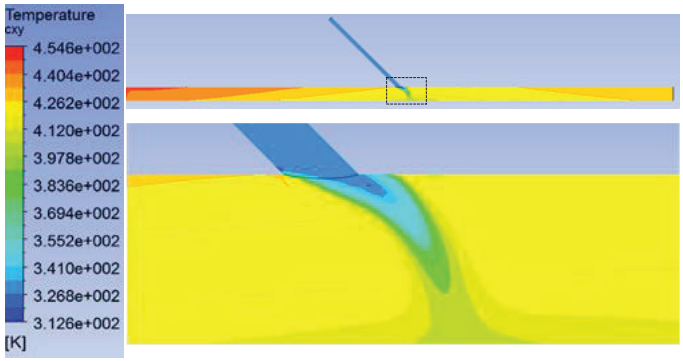

(a) Overall view of temperature distribution of the longitudinal section

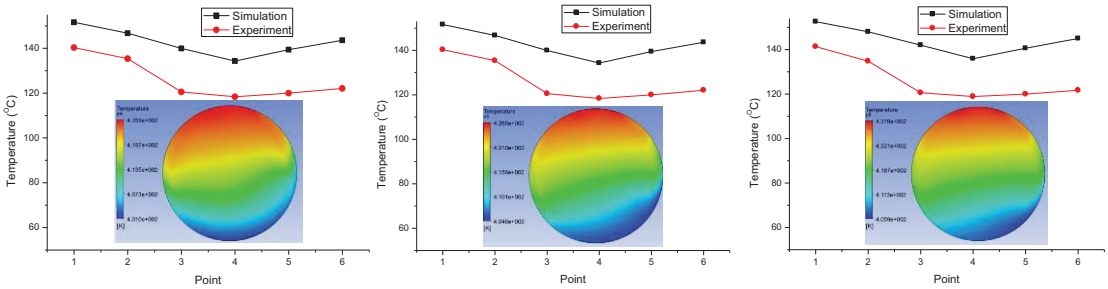

(b) Plane 1 (c) Plane 2 (d) Plane 3

Fig.6. Temperature profile and comparison against the experiment at M_R=0.1

The numerical data agree well with that of the experiment. When M_R is relatively small(M_R<0.3), the

down point of Plane 4 is influenced by the sub-cooled water from the branch pipe more than high temperature water from the main pipe, hence the temperature of which is relatively small. And the mixing in the test section is impinging jet. As M_R increases, temperature rises fast because the injection nozzle's influence over the down point reduces. It indicates that the water from the injection nozzle cannot reach the down point. This is when it turns from impinging jet to turn jet. When M_R is relatively big (M_R>1.8), the temperatures at the up and the down points keep constant values. This is where it turns to re-attached jet. At last, when M_R>4, the temperature of the down point becomes larger as the branch pipe water can hardly touch the down point, which is called wall jet.

As the transition points mainly result from the test section with a 45 degree between the safety injection nozzle and cold leg, these transition points may differ from Seyed Mohammad Hosseini's conclusions.

The temperature profile and comparison against the experiment at M_R=0.1, 1.93 and 4.97 is presented from fig.6 to fig.8. The first part is the overall longitudinal section and the enlarged view of the mixing area, and the others are the temperature distribution at the 6 points of the plane 1, 2 and 3, respectively. As the MR number varies from 0.1 to 4.92, the thermal stratification is clearly seen according to the temperature profile. The position of each point is listed at chapter 3.2. The temperature of point 4 is the lowest of the 6 points considering it being the lowest position of the 3 planes at 3 different working conditions.

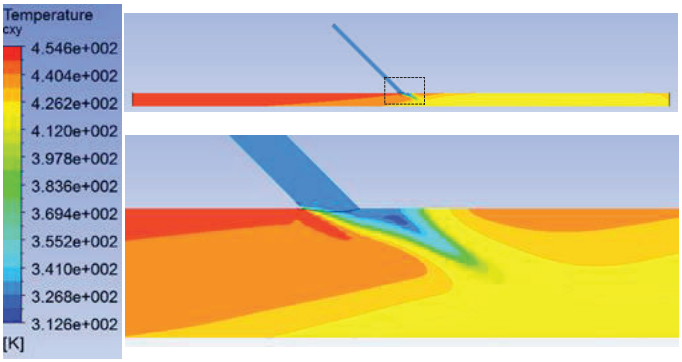

(a) Overall view of temperature distribution of the longitudinal section

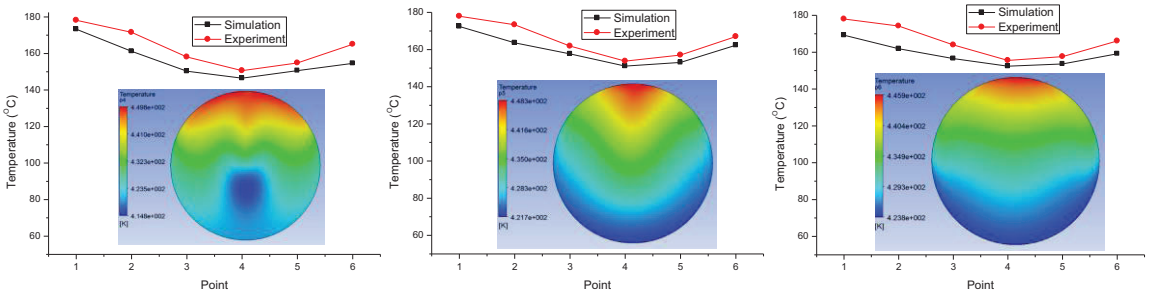

(b) Plane 1 (c) Plane 2 (d) Plane 3

Fig.7. Temperature profile and comparison against the experiment at M_R=1.93

When M_R=0.1, the velocity of the branch pipe is relatively big compared to that of the main pipe. The temperature of the longitudinal section along the axial line shows that even before the mixing area, there exists a large under-main-pipe-temperature area, which indicates that there can be a large zone of backflow before the mixing. It also suggests that under this low M_R number, the flow from the branch pipe comes down directly into the main pipe down-wall. And the gap between the simulation and the experiment is rather big. However, the temperature contours of the three planes have shown great similarity.

When M_R=1.93, the velocity of the branch pipe is comparable to that of the main pipe. The temperature of the longitudinal section along the axial line shows that even before the mixing area, there exist a smaller under-main-pipe-temperature area, which indicates the backflow may occur in that area. And the gap between the simulation and the experiment is smaller than that case of M_R=0.1.

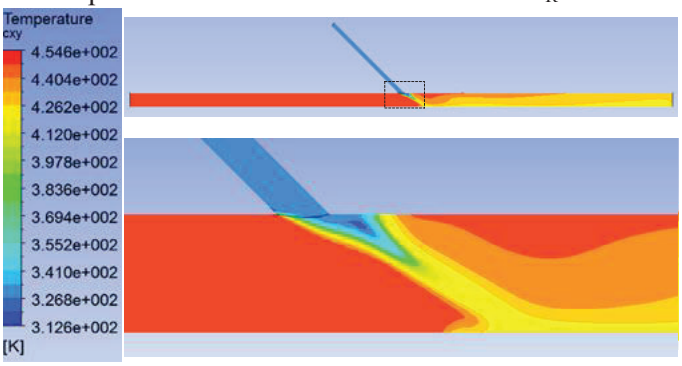

(a) Overall view of temperature distribution of the longitudinal section

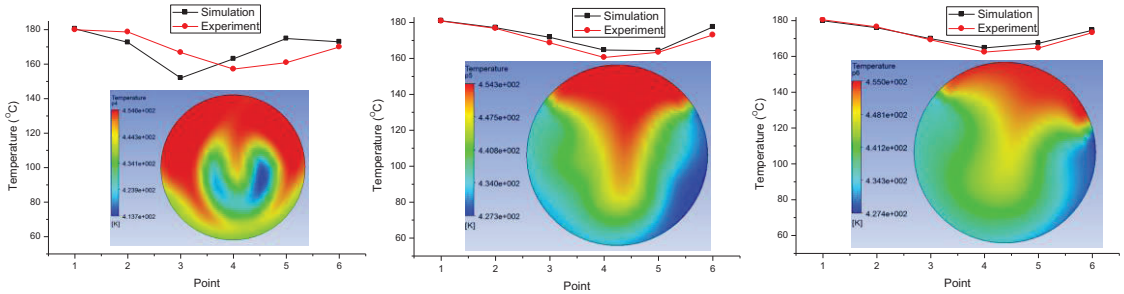

(b)Plane 1 (c) Plane 2 (d) Plane 3

Fig.8. Temperature profile and comparison against the experiment at M_R=4.97

When M_R=4.97, the velocity of the main pipe is dominant. The temperature of the longitudinal section along the axial line does not show any under-main-pipe-temperature area, which indicates that there can be no zone of backflow before the mixing. And the gap between the simulation and the experiment is the smallest. And the temperature contours of the three planes differs, which serves as an indication that the temperature variation is rather big in this case.

Anyway, the temperature distributions of the thermal mixing were simulated and the results have been compared with the experiment data. And the results agree well with the experiment.

4.2 Stratified phase simulation

In the experiment, to make sure that the steam from the main pipe is saturated, the fluid from the main pipe is not 100% pure steam but saturated steam with some saturation water. It has made a comparison between the simulations and the experiment very difficult. For that reason, some features like the temperature field are not compared with the experiment.

When the water from the branch pipe is at a constant velocity of 0.037m/s, a comparison of the steam velocity varying from 1.7m/s to 8.5m/s is made. At a lower steam velocity, the water from the branch pipe went straight down to the main pipe wall whereas at a higher steam velocity, the steam from the main pipe pushes the water just came from the intersection far and thus creating a much larger mixing area. Note that the steam might also go up to the branch pipe and condensed on the water surface as shown in Fig.8. Two reasons can be attributed to this:

(a) The angle of the branch and main pipe is 45 ^{O}C, water has a relatively larger density than steam which makes it much easier to go up to the branch.

(b) The water velocity is much smaller than that of the steam.

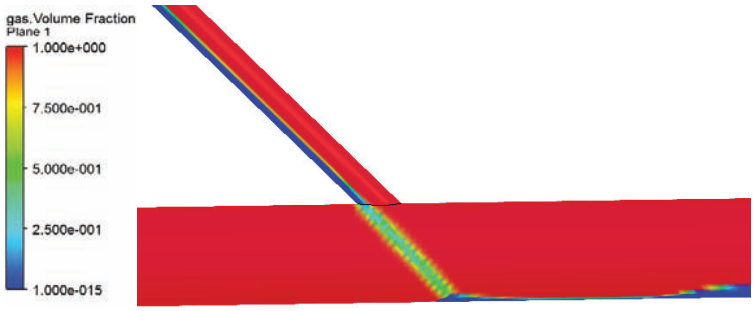

(a) Vg,s=1.7m/s

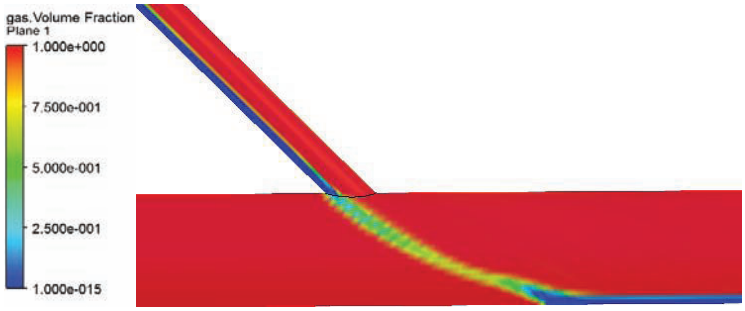

(b) Vg,s=8.5m/s

Fig.9. Gas Volume Fraction at cross-section with different superficial steam velocity

Since the Euler-Euler method treats the gas and liquid in the same grid and they can only be distinguished by the volume fraction (the available minimum volume fraction for each phase is $1.0*10^{-15}$), so the liquid shown above is the mesh with a higher liquid volume fraction of 0.02. As Fig.10 depicts, the temperature went up as the water keeping mixing with the steam. When the steam velocity is relatively high, the water temperature tends to rise faster than that of the low steam velocity.

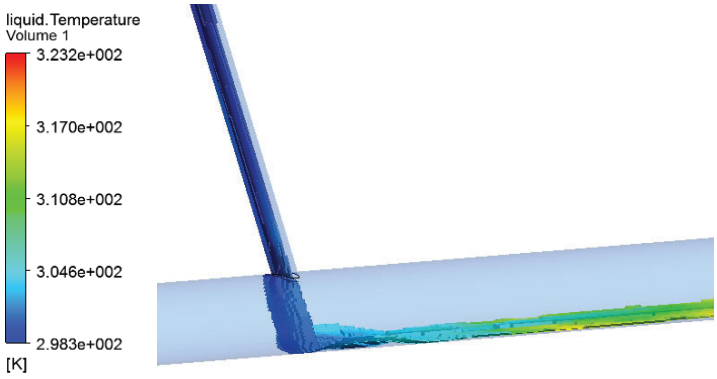

(a) Vg,s=1.7m/s

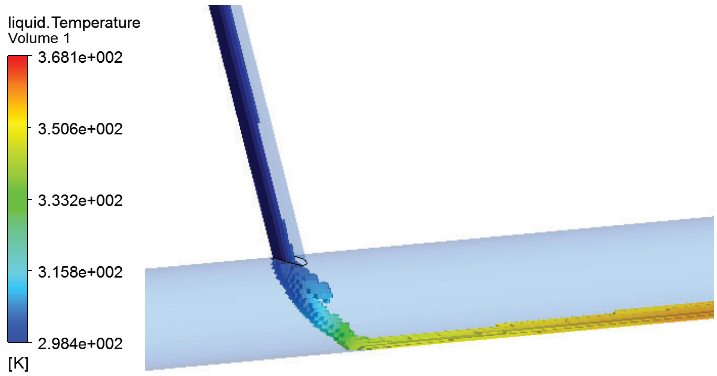

(b)Vg,s=8.5m/s

Fig.10. Liquid Temperature with different superficial steam velocity

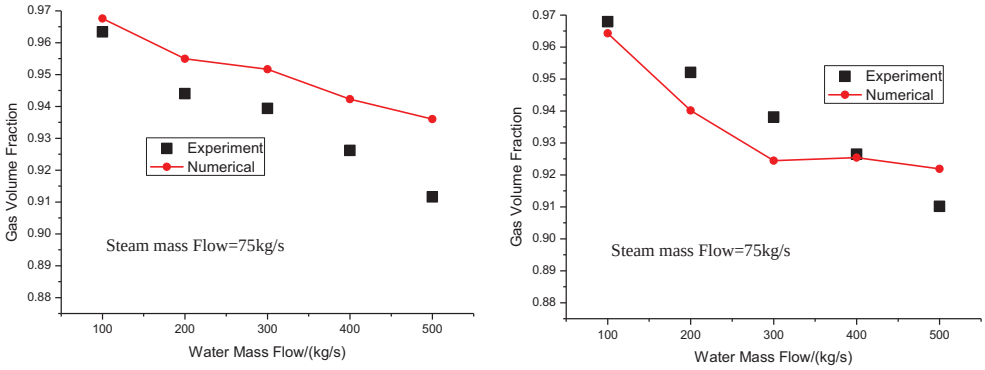

Fig.11. Steam volume fraction varying with water mass flow

Fig.11 shows the gas volume fraction changing when the incoming steam mass flow rate varying from 0.006944kg/s to 0.034722kg/s. it is quite clear that though there can be difference between the experimental results and the numerical results, the trend of the gas volume fraction varying with the water mass flow is the same. With the water mass flow increasing, the gas volume fraction deceases, which means more steam condensates and becomes liquid. From fig.12, it can be concluded that the results of a smaller water mass flow somehow agrees with the experiment better than that of a bigger water mass flow. And with the water mass flow increasing, the gas volume fraction decreases.

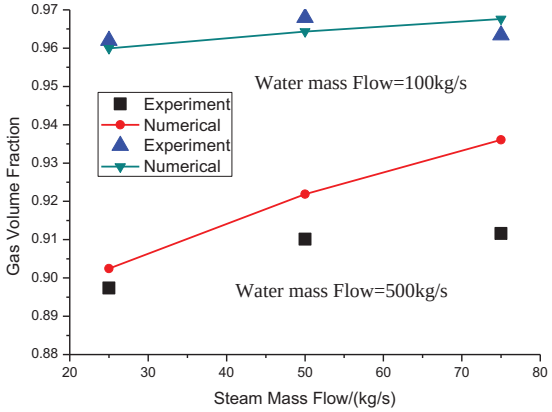

Fig.12. Steam volume fraction varying with steam mass flow

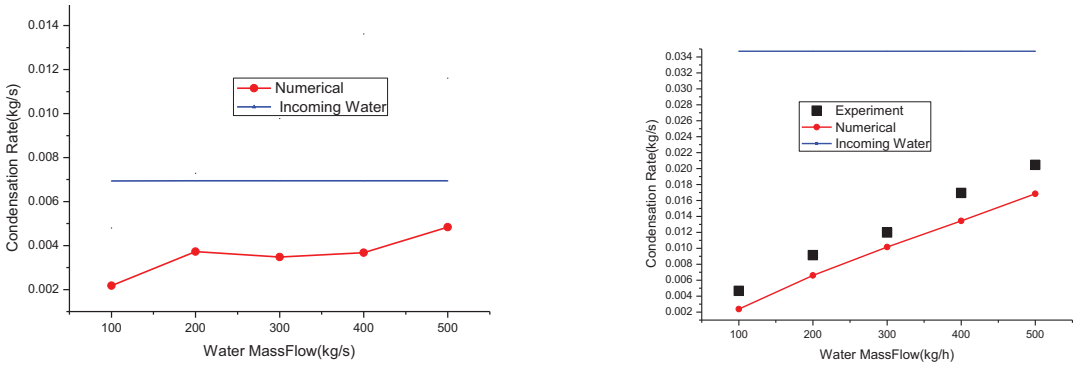

Fig.13. Condensation rate varying with water mass flow

Fig.13 shows the condensation rate when the incoming steam mass flow rate varies from 0.006944kg/s to 0.034722kg/s. For some reasons, the experiment data of the former one is not given (the mass flow rate of the steam is relatively small so the results are not completely convincing). However, the trend can be correct in some way. As the water mass flow becomes larger, the condensation rate increases. At the steam mass flow rate being 0.034722kg/s, the numerical results agree well with the experiment. The reason that the experiment data are somehow larger than that of the simulation that may be that in the experiment the steam is not 100% pure but still mixed with a little saturation water as mentioned before.

5 CONCLUSIONS

A comprehensive computational fluid dynamic model has been adopted for horizontal two-phase pipe flows and single phase flow. And the simulated results are compared with the experimental data. For the single phase thermal mixing phenomenon, the calculated results obtained with k-ε models agree well with test data.

For single phase, temperature variation with MR number of a single phase is provided and compared with the experiment. Note that the k-ε is applied here. Four kinds of jets patterns can be derived indirectly from the temperature distribution. More detailed temperature data of 6-point-plane are also provided. Temperature fluctuations occur only near the wall of main pipe.

For stratified flow, the AIAD model and one heat transfer coefficient has been adopted to simulate the steam-water stratified flow. It is noticed that the steam may also went up to the branch pipe and condensed on the water surface. With a larger steam mass flow, the larger temperature will be much larger at the outlet. Also the gas volume fraction rises with the water mass flow when the steam mass flow is constant and decreases with the water mass flow. With a larger steam mass flow, the larger temperature will be much larger at the outlet. Also the condensation rate rises with the water mass flow when the steam mass flow is constant. It is applicable to model the stratified flow with the AIAD model and heat transfer model.

REFERENCE

[1] 2009. ANSYS CFX 12.0 User Manual. ANSYS.

[2] Naik-Nimbalkar, V. S.; Patwardhan, A. W.; Banerjee, I. Thermal mixing in T-junctions. Chemical Engineering Science 65 (2010) 5901–5911

[3] Seyed Mohammad Hosseini, Kazuhisa Yuki, Hidetoshi Hashizume, 2008. Classification of turbulent jets in a T-junction area with a 90-deg bend upstream. International Journal of heat and mass transfer 51, 2444-2454

[4] Kamide, H., Igarashi, M., Kawashima, S., Kimura, N., Hayashia, K., 2009. Study on mixing behavior in a tee piping and numerical analyses for evaluation of thermal striping. Nuclear Engineering and Design 239, 58–67.

[5] Frank T, Adlakha M, Lifante C, et al. Simulation Of Turbulent And Thermal Mixing In T-Junctions Using Urans And Scale-Resolving Turbulence Models In Ansys Cfx[J]. Nuclear Engineering & Design, 2010, 240(9):2313–2328.

[6] Hu L W, Kazimi M S. LES benchmark study of high cycle temperature fluctuations caused by thermal striping in a mixing tee[J]. International Journal of Heat & Fluid Flow, 2006, 27(1):54–64.

[7] Deendarlianto, H02hne T, Apanasevich P, et al. Application of a new drag coefficient model at CFD-simulations on free surface flows relevant for the nuclear reactor safety analysis[J]. Annals of Nuclear Energy, 2012, 39(1):70–82.

[8] Vallée C, H02hne T, Prasser H M, et al. Experimental investigation and CFD simulation of horizontal air/water slug flow[J]. Kerntechnik, 2006, 71(3):95-103.

[9] Egorov, Y., 2004. Validation of CFD codes with PTS-relevant test cases. In: 5th Euratom Framework Programme ECORA project

[10] Coste, P. and A. Ortolan, Two-phase CFD PTS validation in an extended range of thermohydraulics conditions covered by the COSI experiment. Nuclear Engineering and Design, 2014. 279(0): p. 158-170.

[11] D. Hughes and R. B. Duffey E. Direct contact condensation and momentum transfer in turbulent separated flows[J]. International Journal of Multiphase Flow, 1991, (5):599-619.

[12] Bartosiewicz, Y., et al., Modeling free surface flows relevant to a PTS scenario: Comparison between experimental data and three RANS based CFD-codes. Comments on the CFD-experiment integration and best practice guideline. Nuclear Engineering and Design, 2010. 240(9): p. 2375-2381.

[13] Hoehne, T., Deendarlianto and D. Lucas, Numerical simulations of counter-current two-phase flow experiments in a PWR hot leg model using an interfacial area density model. International Journal of Heat and Fluid Flow, 2011. 32(5): p. 1047-1056.

[14] Hoehne, T. and J. Mehlhoop, Validation of closure models for interfacial drag and turbulence in numerical simulations of horizontal stratified gas-liquid flows. International Journal of Multiphase Flow, 2014. 62(0): p. 1-16.

[15] Apanasevich, P., et al., Comparison of CFD simulations on two-phase Pressurized Thermal Shock scenarios. Nuclear Engineering and Design, 2014. 266(0): p. 112-128.